

Fermi surface and strong coupling superconductivity in single crystal $\text{NdFeAsO}_{1-x}\text{F}_x$

C. Liu,¹ T. Kondo,¹ M. E. Tillman,¹ R. Gordon,¹ G. D. Samolyuk,¹ Y. Lee,¹ C. Martin,¹ J. L. McChesney,² S. Bud'ko,¹ M. A. Tanatar,¹ E. Rotenberg,² P. C. Canfield,¹ R. Prozorov,¹ B. N. Harmon,¹ and A. Kaminski¹

¹*Ames Laboratory and Department of Physics and Astronomy, Iowa State University, Ames, Iowa 50011, USA*

²*Advanced Light Source, Berkeley National Laboratory, Berkeley, California 94720, USA*

(Dated: March 1, 2022)

We use angle-resolved photoemission spectroscopy (ARPES) to investigate the electronic properties of the newly discovered oxypnictide superconductor, $\text{NdFeAsO}_{1-x}\text{F}_x$. We find a well-defined Fermi surface that consists of a large hole pocket at the Brillouin zone center and a smaller electron pocket in each corner of the Brillouin zone. The overall location and shape of the Fermi surface agrees reasonably well with calculations. The band dispersion is quite complicated with many flat bands located just below the chemical potential. We observe a superconducting gap of 20 meV, which indicates that this system is in the strong coupling regime. The emergence of a coherent peak below the critical temperature T_c and diminished spectral weight at the chemical potential above T_c closely resembles the spectral characteristics of the cuprates.

PACS numbers: 79.60.-i, 74.25.Jb, 74.70.-b

Superconductivity is a spectacular manifestation of quantum mechanics on a macroscopic scale. In most cases this phenomenon can be well understood within the Bardeen-Cooper-Schrieffer theory as phonon mediated pairing of electrons and condensation of the resulting boson gas. All known superconductors that can be understood within this theory have critical temperatures, (below which they become superconducting or T_c) less than $\sim 40\text{K}$ [1]. For over twenty years the only known exception was the cuprate family of high temperature superconductors where superconductivity of unknown mechanism exists up to $\sim 130\text{K}$. Recently, the discovery of superconductivity with a T_c up to 55K in a new class of materials with the general formulae $\text{LnFeAsO}_{1-x}\text{F}_x$ (Ln being the lanthanides La, Sm, Ce, Nd, Pr, and Gd, x being the fluorine doping level) [2, 3, 4] raises interesting questions on whether the mechanism of pairing in these new materials is the same as in the cuprates, or if there is yet another way superconductivity can be established.

There are already a number of different scenarios proposed for the mechanism in this new class of materials. In some theories the superconductivity arises due to the suppression of spin density wave (SDW) ordering between the Γ and M Fermi sheets [5, 6, 7, 8, 9]. For this scenario to work both sheets need to have similar radii. In other classes of theory, flat bands just below the chemical potential are important as they can couple electrons at the Fermi surface via Coulomb or Hund's rule scattering. A prerequisite to understanding the mechanism of superconductivity in these materials is the knowledge of the low lying electronic excitations because these are the states that eventually compose the superconducting condensate. A number of angle integrated photoemission studies are available in the literature [10, 11, 12] on this subject, but as yet no angle resolved data is available that addresses the questions about the low lying electronic excitations. Here we present data from an-

gle resolved photoemission spectroscopy (ARPES) on the Fermi surface, band dispersion and superconducting gap in $\text{NdFeAsO}_{1-x}\text{F}_x$. We find that the Fermi surface consists of a cylindrical hole pocket centered around Γ (0,0,0) and a cylindrical electron pocket at each corner of the Brillouin zone (M points), similar to most calculations [5, 13, 14, 15]. Some band calculations yield also an ellipsoidal Fermi surface around Z (0,0,1) [13, 14]. We did not observe this for the studied photon energies, however we did find a flat top band just below the chemical potential centered at Γ . Even with a very small k_z dispersion, this band could cross the chemical potential and give rise to the ellipsoidal Fermi surface at Z. We observe a superconducting gap of $\Delta = 20$ meV at the Γ hole pocket for $T = 20\text{K}$. This corresponds to $2\Delta/T_c = 8$ and indicates that this system is in the strong coupling regime. We note that this ratio is similar to that of the cuprate family of high temperature superconductors. The emergence of the coherent peak below T_c and diminished spectral weight at the chemical potential above T_c closely resembles the spectral characteristics of the cuprates.

High pressure synthesis of samples with the nominal composition of $\text{NdFeAsO}_{0.9}\text{F}_{0.1}$ was carried out in a cubic, multianvil press, with an edge length of 19 mm from Rockland Research Corporation. Stoichiometric amounts of NdFe_3As_3 , Nd_2O_3 , NdF_3 and Nd were pressed into a pellet with a mass of approximately 0.5 g and placed inside of a BN crucible with an inner diameter of 5.5 mm. The synthesis was carried out at a pressure of 3.3 GPa. The temperature was increased, over one hour, from room temperature to 1350 - 1400°C and then held there for 8 hours before being quenched to room temperature. The pressure was then released and the sample was removed mechanically. This synthesis produced a high density pellet that contained large grains (up to $300 \times 200 \mu\text{m}$ in cross section) of superconducting ($T_c \sim 53$ K) $\text{NdFeAsO}_{0.9}\text{F}_{0.1}$ as well as non-superconducting

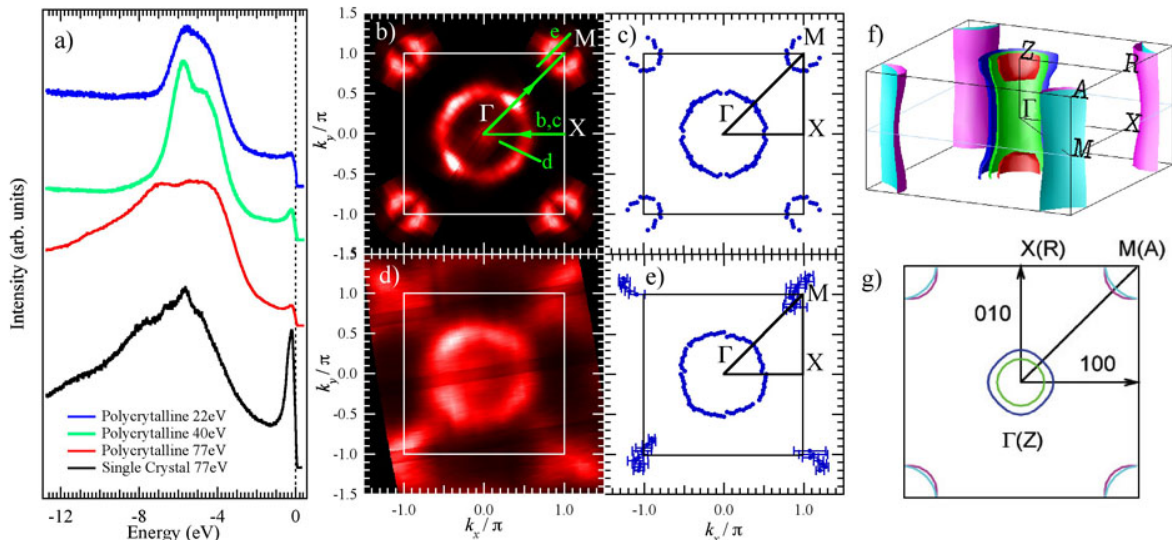


FIG. 1: (color) Measured and calculated Fermi surface of $\text{NdFeAsO}_{1-x}\text{F}_x$ and NdFeAsO respectively. **a**, Angle integrated spectra from polycrystalline and single crystal samples for selected photon energies. **b**, Fermi surface map - intensity of the photoelectrons integrated over 20 meV about the chemical potential obtained with 22 eV photons at $T = 70\text{K}$. The areas of bright color mark the locations of the Fermi surface. Green lines and arrows mark the location of the selected cuts for Figure 2a-b. **c**, The locations of the Fermi crossings extracted from the raw data by fits to the momentum distribution curves (MDCs). **d**, same data as in **b**) but obtained with 77 eV photons. **e**, same data as in **c**) but obtained with 77 eV photons. **f**, 3-dimensional FS of NdFeAsO obtained from FLAPW calculations. **g**, A FS cross-section at $k_z = 0$ ($X\text{-}\Gamma\text{-M}$ plane) obtained by FLAPW calculations.

NdFeAsO . In addition there are inclusions of FeAs and Nd_2O_3 . Magneto optical measurements [16] indicate that on average the samples are over 50% superconducting. The single crystals were mechanically extracted from the pellet. They were then mounted on an Al pin using UHV compatible epoxy and cleaved *in situ* yielding flat mirror-like surface. The data was acquired at the PGM beamline of the Synchrotron Radiation Center, using a Scienta 2002 analyzer and at the Advanced Light Source using beamline 12.0.1 equipped with a Scienta 4000 analyzer. The energy and angular resolution were set at 30 meV and 0.5 degree, respectively. The beam profile on the sample was slightly elliptical, with a mean diameter smaller than $100\mu\text{m}$. The photoelectron energy corresponding to the chemical potential was determined by measuring spectra from polycrystalline aluminium in electrical contact with the sample. Measurements carried out on several samples yielded similar results for the band dispersion and Fermi surface. Our full-potential linearized plane wave (FLAPW) calculation [17] used the local density approximation(LDA) [18], and the experimental lattice constants [19] for the undoped parent compound NdFeAsO . For the internal parameters, since there is no available experimental data we take atomic positions from PrFeAsO [19] and optimize As position by total energy minimization that results in $z_{\text{As}} = 0.639c$.

Measurements on single crystals are essential for an

accurate determination of the electronic structure. The presence of multiple phases in polycrystalline samples can often contaminate the pristine spectra. As an example we plot in figure 1a a comparison of the photoemission data from polycrystalline samples and angle integrated measurements from single crystals. The strong intrinsic peak just below the chemical potential is very strongly suppressed in the polycrystalline samples. A common method for illustrating the topology of the Fermi surface is to plot the ARPES intensity at the chemical potential as a function of momentum [20, 21]. In Fig. 1b,d we plot the ARPES intensity integrated within 20 meV about the chemical potential from data obtained using 22eV and 77eV photons. The brightest areas in these plots indicate high photoelectron intensity and therefore approximate to the location of the Fermi surface. To obtain more accurate information we have extracted the exact locations of the Fermi momentum from momentum distribution curves (MDCs) using a procedure described elsewhere[21] and plot them in panels 1c and 1e. Our data show that indeed this system has a Fermi surface that consists of two main contours: a larger one centered at Γ (0,0) and a smaller one centered at the corners of the Brillouin zone. For comparison we plot the 3-dimensional (3D) Fermi surfaces based on FLAPW band calculations for fluorine-free NdFeAsO in figure 1f. A 2D cut at Γ ($k_z = 0$) is shown in figure 1g. We note that there are

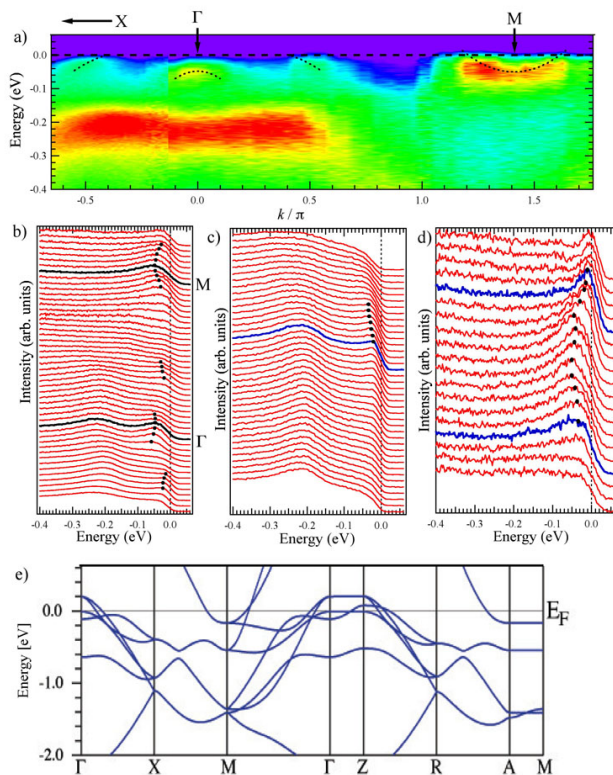


FIG. 2: (color) Measured and calculated band dispersion. Locations of the cuts are indicated by green lines in figure 1(b). **a**, Measured ARPES intensity along the X- Γ -M direction ($T = 70$ K). Black dashed curves are guides to the eye. **b** Energy distribution curves (EDCs) for data in panel a) at $T = 70$ K. **c** and **d**, EDCs ($T = 70$ K) in the directions shown in figure 1b). Blue curves mark the Fermi crossing momenta k_F . **e**, Band dispersion along the symmetry directions for fluorine-free NdFeAsO obtained from FLAPW calculations.

both similarities and differences between the data and calculations. Overall the calculation predicts Fermi surface sheets centered at Γ and M, in agreement with our measurements. The main difference between theory and experiment is the number of FS sheets and their relative size. According to calculation there should be two sheets at each symmetry point. It is quite possible that the separation between the sheets is smaller than the calculated result and not sufficient to resolve in the experiment. A second disagreement is in the size of the Γ -pocket and the ratio of its radius to that of the M-pocket. This poses a significant challenge for models relying on nesting between the Γ and M Fermi surface sheets and can be possibly reconciled when strong electron correlations are taken into account.

The band dispersion along selected cuts (indicated by green arrows in figure 1b) is shown in figure 2. Panel 2a shows the intensity map along the X- Γ -M symmetry line. Bright areas on this graph mark the locations of

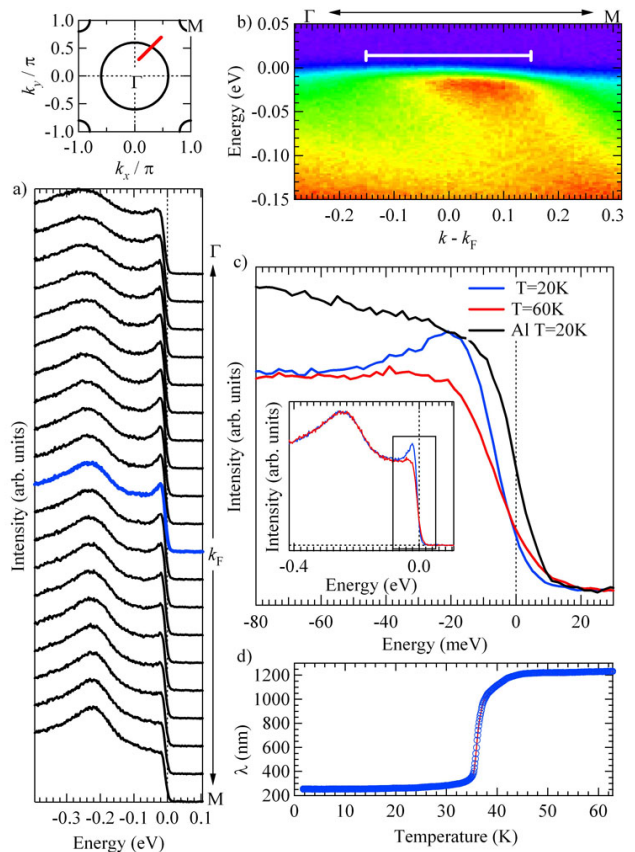


FIG. 3: (color) Superconducting gap at the Γ pocket, location marked in the upper-left inset. **a**, EDCs along the cut. Blue line indicates the EDC at the Fermi momentum. **b**, Intensity map along this cut with a clearly visible dispersion and back bending of the band close to Fermi energy E_F caused by the superconductivity. The white line marks the range of momenta for which the EDCs are plotted in panel a). **c**, Magnified low binding energy region from inset, where EDCs at $T = 60$ K and $T = 20$ K are plotted. Black curve is a reference spectra from polycrystalline Al. **d**, The penetration depth data measured using the Tunneling Diode Resonator technique on the same crystal after the ARPES measurement. A strong superconducting signal is shown.

the bands. From these data we can identify the topology of the main Fermi surface components. The Fermi surface centered at Γ is hole-like, i.e., the unoccupied states are on the top of this band. In contrast, the Fermi surface centered at M is electron-like with the bottom of the band located at ~ 50 meV below the chemical potential. In addition to these two conduction bands, there are also two very prominent fully occupied bands for this particular value of k_z . The tops of both are centered at Γ . The first is located just 50 meV below the chemical potential. We speculate that this might be the band responsible for the ellipsoidal pocket at Z, since even a small amount of k_z dispersion would bring its top above the chemical potential. The second band has a rather flat top which

is located at ~ 200 meV below the chemical potential. This band is most likely responsible for the strong peak observed in angle integrated measurements [10, 11, 12]. EDCs for the above data are shown in panel b. The dispersion of the peaks in this plot agrees with the above description of the Fermi surface topology. The band dispersion close to the chemical potential for the Γ pocket and M pocket are plotted in panels 2c and 2d respectively. The location of the Fermi momenta are marked by blue solid lines. In panel 2e the calculated band structure at the high symmetry points for fluorine-free NdFeAsO is presented for comparison.

We now proceed to discuss the measurements of the superconducting gap in this material. The EDCs and ARPES intensity along a selected cut at the Γ pocket are shown in Fig. 3a-b. The Fermi momentum was determined using the peak position of the MDCs and it is marked in blue. The inset of panel (c) shows the EDCs below (red) and above (blue) T_c , whereas in the enlarged panel we plot the magnified part of EDCs close to the chemical potential. The black curve is a chemical potential reference measured using polycrystalline aluminium in electrical contact with sample. The peak of the EDC above T_c is very broad and its leading edge is slightly shifted (~ 10 meV) towards higher binding energies, which indicates the possible existence of a pseudogap. At present we do not have extensive temperature dependent data to definitely confirm whether these effects are similar to the pseudogap observed in the cuprates. We have performed these measurements with varying photon flux and confirmed that this shift is not due to charging effects. Below T_c the spectrum changes quite dramatically - a coherent peak develops at a binding energy of ~ 20 meV which roughly corresponds to the value of the superconducting gap. In addition, a characteristic back-bending of the band is observed in the dispersion (panels 3a,b) which arises due to particle-hole mixing in the superconducting state. The spectral signatures of the superconducting transition are strikingly similar to the ones widely reported in cuprates. Namely, below T_c a sharp peak appears, violating the conservation of low energy spectral weight. This additional weight in the case of the cuprates correlates reasonably well with the superfluid density [22, 23]. Following the ARPES experiments we have performed measurements of the temperature dependence of the penetration depth on the same crystal. Due to the small size of the crystals ($200 \times 200 \times 30 \mu\text{m}$),

the measurements were performed using a very sensitive Tunneling Diode Resonator technique [24]. Penetration depth data confirms that the crystals measured by ARPES are indeed superconducting.

We are grateful for useful discussions with Jörg Schmalian. We thank Helen Fretwell for useful remarks and corrections. Work at Ames Laboratory was supported by the Department of Energy - Basic Energy Sciences under Contract No. DE-AC02-07CH11358. The Synchrotron Radiation Center is supported by NSF DMR 9212658. ALS is operated by the US DOE under Contract No. DE-AC03-76SF00098.

-
- [1] W. L. McMillan, Phys. Rev. **167**, 331 (1968)
 - [2] Yoichi Kamihara, Takumi Watanabe, Masahiro Hirano, and Hideo Hosono, J. Am. Chem. Soc. **130**, 3296 (2008).
 - [3] Hiroki Takahashi *et al.*, Nature(London) **453**, 376 (2008)
 - [4] Ren Zhi-An *et al.*, Chin. Phys. Lett. **25**, 2215 (2008).
 - [5] J. Dong *et al.*, arXiv:0803.3426 (2008)
 - [6] Zheng-Yu Weng, arXiv:0804.3228 (2008)
 - [7] Clarina de la Cruz *et al.*, arXiv:0804.0795 (2008)
 - [8] Ying Ran, Fa Wang, Hui Zhai, Ashvin Vishwanath and Dung-Hai Lee, arXiv:0805.3535 (2008)
 - [9] Fa Wang, Hui Zhai, Ying Ran, Ashvin Vishwanath and Dung-Hai Lee, arXiv:0805.3343 (2008)
 - [10] T. Sato *et al.*, J. Phys. Soc. Jpn. **25**, in press (2008).
 - [11] Xiaowen Jia *et al.*, arXiv:0806.0291 (2008)
 - [12] Haiyun Liu *et al.*, arXiv:0805.3821 (2008)
 - [13] S. Lebegue, Phys. Rev. B **75**, 035110 (2007).
 - [14] D.J. Singh and M.H. Du, arXiv:0803.0429 (2008)
 - [15] Gang Xu *et al.*, Europhys. Lett. **82**, 67002 (2008).
 - [16] R. Prozorov, M. E. Tillman, E. D. Mun and P. C. Canfield, arXiv:0805.2783 (2008)
 - [17] P. Blaha, K. Schwarz, G. K. Madsen, D. Kvasnick and J. Luitz, *WIEN2K, An augmented Plane wave + Local Orbitals Program for Calculation Crystal Properties.* (K. Schwarz, TU Wien, Austria, 2001) ISBN 3-9501031-1-2
 - [18] J. P. Perdew and Y. Wang, Phys. Rev. B **45**, 13244 (1992), J. Alloys Compd., **302**, 70 (2000)
 - [19] P. Quebe, L. J. Terbüchte and W. Jeitschko, J. Alloys Compd., **302**, 70 (2000)
 - [20] H. M. Fretwell *et al.*, Phys. Rev. Lett. **84**, 4449 (2000)
 - [21] J. Mesot *et al.*, Phys. Rev. B **63**, 224516 (2001)
 - [22] A. V. Fedorov *et al.*, Phys. Rev. Lett. **82**, 2179 (1999).
 - [23] D. L. Feng *et al.*, Science **289**, 277 (2000).
 - [24] R. Prozorov and R. W. Giannetta, Superc. Sci. Tech. **19**, R41 (2006).